Differential Peptide Dynamics Is Linked to Major Histocompatibility Complex Polymorphism*⑤

Thomas Pöhlmann‡§, Rainer A. Böckmann¶§‖, Helmut Grubmüller¶, Barbara Uchanska-Ziegler**, Andreas Ziegler**, and Ulrike Alexiev‡ ‡‡

*From the ‡Department of Physics, Freie Universität Berlin, Arnimallee 14, D-14195 Berlin, Germany, the ¶Theoretical and Computational Biophysics Department, Max-Planck-Institut für Biophysikalische Chemie, D-37077 Göttingen, Germany, and the **Institut für Immungenetik, Charité-Universitätsmedizin Berlin, Humboldt-Universität zu Berlin, Spandauer Damm 130, D-14050 Berlin, Germany*

Peptide presentation by major histocompatibility complex (MHC) molecules is of central importance for immune responses, which are triggered through recognition of peptide-loaded MHC molecules (pMHC) by cellular ligands such as T-cell receptors (TCR). However, a unifying link between structural features of pMHC and cellular responses has not been established. Instead, pMHC/TCR binding studies suggest conformational and/or flexibility changes of the binding partners as a possible cause of differential T-cell stimulation, but information on real-time dynamics is lacking. We therefore probed the real-time dynamics of a MHC-bound nonapeptide (m9), by combining time-resolved fluorescence depolarization and molecular dynamics simulations. Here we show that the nanosecond dynamics of this peptide presented by two human MHC class I subtypes (HLA-B*2705 and HLA-B*2709) with differential autoimmune disease association varies dramatically, despite virtually identical crystal structures. The peptide dynamics is linked to the single, buried polymorphic residue 116 in the peptide binding groove. Pronounced peptide flexibility is seen only for the non-disease-associated subtype HLA-B*2709, suggesting an entropic control of peptide recognition. Thermodynamic data obtained for two additional peptides support this hypothesis.

MHC[1] class I molecules consist of a highly polymorphic transmembrane heavy chain that is non-covalently associated with a light chain, β_2-microglobulin (β_2m) (1). Peptidic fragments of self- or non-self-proteins are loaded on MHC class I molecules in the endoplasmatic reticulum, followed by transport to the cell surface. Recognition of these peptide-loaded MHC molecules (pMHC) by cellular ligands such as T-cell receptors (TCR) triggers an immune response. Despite their inherent cross-reactivity (2), TCR must be able to discriminate between foreign antigens and the huge number of self-peptides to avoid autoreactivity. The biological activity of T-cells has been correlated with pMHC-TCR binding kinetics (3–5), but a comprehensive link between T-cell activation or desensitization with structural features of the TCR or pMHC has still not been established (5–9). To solve this puzzle, a closer look at the underlying *dynamical* processes at the atomic level is mandatory (5, 6).

To that aim, we have combined site-directed fluorescence labeling, picosecond time-resolved fluorescence depolarization, and molecular dynamics (MD) simulations. Two human leukocyte antigen (HLA) class I subtypes were compared, which are differentially associated with the autoimmune disease ankylosing spondylitis (AS). HLA-B*2705 and B*2709 differ only in one amino acid at position 116 at the floor of the peptide binding groove (Asp-116 in the AS-associated subtype B*2705 and His-116 in the B*2709 subtype, which lacks the AS association) (10). High resolution x-ray structures of the soluble ectodomains of both subtypes in complex with the peptide m9 (GRFAAAIAK) have been determined previously and are virtually indistinguishable (11). We demonstrate here that the dynamics of this peptide varies dramatically between the subtypes, and a pronounced peptide flexibility is seen only for one of the subtypes. The differential peptide flexibility explains the difference in the entropic component of the free energy between the subtypes at physiological temperature, suggesting an entropic control of peptide recognition. Additional thermodynamic data for two self-peptides support this hypothesis.

EXPERIMENTAL PROCEDURES

Protein Preparation—Complexes of HLA-B27 with the model peptide m9, and the self-peptides TIS and pVIPR, were prepared as described previously (11). The m9-C6-LY (GRFAAC(LY)IAK), TIS-C6-LY (RRLPI C(LY)SRL), and pVIPR-C8-LY (RRKWRRWC(LY)L) peptides were from Biosynthan. HLA complexes were refolded from 6 M urea in the presence of the respective peptide. After size exclusion chromatography, the concentrations of the HLA-B27:peptide complexes in 10 mM phosphate buffer, pH 7.5, 150 mM NaCl were adjusted for the experiments using the absorption band of Lucifer Yellow ($\lambda_{max} = 426 \pm 2$ nm) to $A_{426} = 0.02$ OD. The fluorescence emission maximum of Lucifer Yellow covalently bound to the peptides is $\lambda_{max} = 532 \pm 1$ nm.

Time-resolved Fluorescence Spectroscopy—The fluorescence anisotropy decays were measured employing a tunable Ti:sapphire laser/microchannel plate based single-photon counting apparatus with pico-

---

⑤ The on-line version of this article (available at http://www.jbc.org) contains supplemental Figs. S1–S4 and Table S1.

§ These authors contributed equally to the work.

‖ Present address: Dept. for Biochemistry, Universität Zürich, Winterthurerstrasse 190, CH-8057 Zürich, Switzerland.

‡‡ To whom correspondence should be addressed. Tel.: 49-30-838-55157/56141; Fax: 49-30-838-56299; E-mail: alexiev@physik.fu-berlin. de.

[1] The abbreviations used are: MHC, major histocompatibility complex; pMHC, peptide-loaded MHC; β_2m, β_2-microglobulin; TCR, T-cell receptor; MD simulations, molecular dynamics simulations; HLA, human leucocyte antigen; AS, ankylosing spondylitis; m9, peptide GRFAAA-IAK; LYIA, Lucifer Yellow iodoacetamide; m9-C6-LY, peptide GRFAA(C-LY)IAK labeled in position 6 with LYIA; TIS, peptide RRLPIFSRL; TIS-C6-LY, peptide RRLPI(C-LY)SRL labeled in position 6 with LYIA; pVIPR, peptide RRKWRRWHL; pVIPR-C8-LY, peptide RRKWRRW(C-LY)L labeled in position 8 with LYIA; CTL, cytotoxic T-cell.

FIG. 1. **Time-resolved fluorescence anisotropy decays and representative conformations of the bound m9 peptide.** Anisotropy time courses, fits (supplemental Table S1) and their residues (*insets*) of LYIA (*green*) and peptide-m9-C6-LY (*red*) (*A*), B*2705:m9-C6-LY (*blue*), and B*2709:m9-C6-LY (*red*) at 20 °C (*B*) and at 37 °C (*C*). Conditions: 10 mM phospate buffer, pH 7.5, 150 mM NaCl. The excitation was at 430 nm. The fluorescence emission was detected after passing through a cut-off color glass filter OG475. *D*, Perrin plot for the estimation of molecular volumes from the slowest rotational correlation time. The effective hydrodynamic diameter of 57 ± 3 Å is in very good agreement with the average diameter of ~60 Å from the crystal structures (11) (*inset*). *E*, crystal (*gray*) and representative m9 conformations of three clusters from a principal component analysis (colored as described under "Results and Discussion") of HLA-B*2709:m9. *F*, projection of the HLA-B*2709 trajectory on the first two eigenvectors from the principal component analysis. Three distinct clusters can be identified (*diamonds*, *X* flags the x-ray structure). *G*, HLA-B*2709 in ribbon and in protein surface representations. Shown are two conformations of the m9 peptide (*space-filled*).
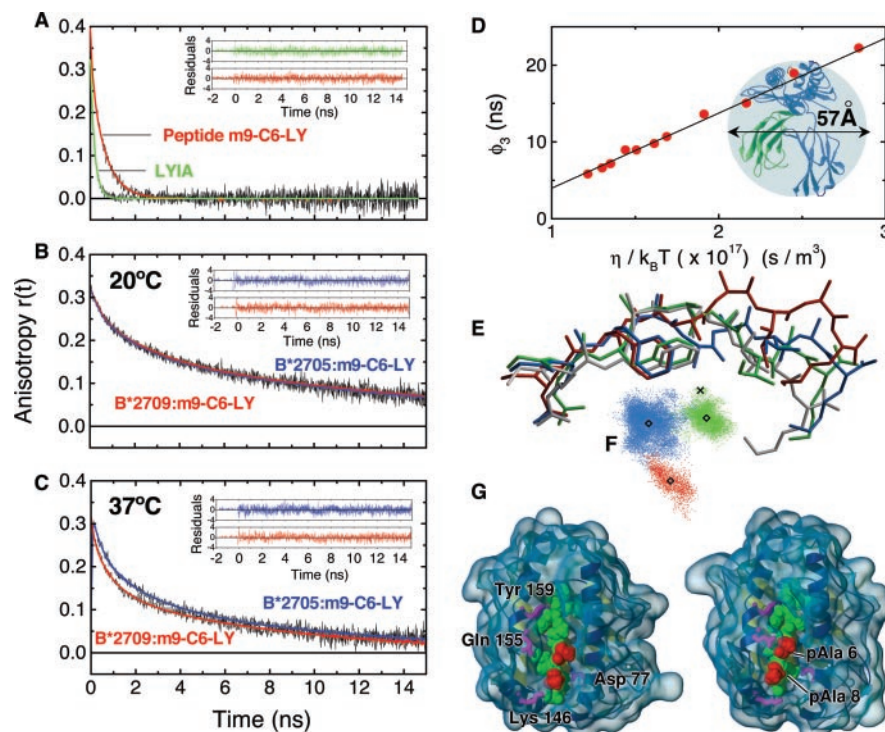
second time resolution (12). The fluorescence decay profiles ($I_\parallel(t)$ and $I_\perp(t)$) and the time-resolved anisotropy as given by the following equation,

$$r(t) = \frac{I_\parallel(t) - I_\perp(t)}{I_\parallel(t) + 2I_\perp(t)} \qquad \text{(Eq. 1)}$$

were analyzed using the software package Global Unlimited V2.2 (Laboratory for Fluorescence Dynamics, University of Illinois). The time course of the fluorescence (supplemental Fig. S1) was fitted with a sum of exponentials (Equation 2).

$$I(t) = \sum_{i=1} \alpha_i e^{-t/\tau_i} \qquad \text{(Eq. 2)}$$

The anisotropy decay was fitted with the model function (Equation 3).

$$r(t) = \sum_{i=1}^{n} \beta_i e^{-t/\phi_i} \qquad \text{(Eq. 3)}$$

The instrumental response function of the system was ~40 ps (FWHM) at a channel width of 5 ps.

Thermally Induced Peptide Dissociation and HLA-B27 Complex Unfolding—The mole fraction of bound peptide molecules and the fraction of peptides free in solution were monitored directly by steady-state anisotropy, as the fluorescence quantum yield of the attached fluorophore did not change upon peptide binding for m9-C6-LY (supplemental Fig. S2). For pVIPR, the fluorescence quantum yield of Lucifer Yellow changes upon peptide dissociation and the change in fluorescence intensity was used to follow peptide dissociation.

The anisotropy data were fitted to the following equation using the least square method assuming a two-state transition (13),

$$r = \frac{r_{0b} + s_b T + [r_{0d} + s_d T]\exp((-\Delta H^0_p + T\Delta S^0_p)/RT)}{1 + \exp((-\Delta H^0_p + T\Delta S^0_p)/RT)} \qquad \text{(Eq. 4)}$$

with

$$T_m = \Delta H^0_p / \Delta S^0_p . \qquad \text{(Eq. 5)}$$

This equation involves six fitting parameters, the fluorescence anisotropy of the peptide in the bound state, r_{0b}, and of the peptide in the unbound state, r_{0d}, at the reference temperature, the temperature dependence of the polarization of the peptide bound state, s_b, and of the peptide unbound state, s_d, the enthalpy change, ΔH^0_p, and the entropy

change, ΔS^0_p, for the two state unfolding reaction. r_{0d} and s_d were determined from the temperature dependence of the peptide free in solution. T_m is the transition temperature.

HLA-B27 complex unfolding was followed by the change in the tryptophan fluorescence intensity at the blue (320 nm) and red (360 nm) side of the tryptophan emission band. T_m was determined from the first derivatives of the denaturation curves. Comparison of the T_m from tryptophan fluorescence with the T_m for unfolding determined by CD (14) shows a good agreement for B*2705:m9 (CD: ~63 °C) and for B*2709:m9 (CD: ~49 °C), indicating that the modification with Lucifer Yellow does not change the thermodynamic properties of the respective complex.

Molecular Dynamics Simulations—As start structures, HLA-B*2709 and HLA-B*2705 subtypes complexed with m9 were taken (Protein Data Bank entries 1K5N and 1JGE at 1.09 Å and 2.10 Å, respectively (11)). The simulations were performed in a periodic box (8.9 × 8.3 × 10.0 nm); the structures were solvated with 21,904 and 22,406 TIP4 (15) water molecules, corresponding to a water shell thickness of at least 1.4 nm around the protein, adding up to simulation sizes of more than 94,000 atoms (supplemental Fig. S3).

Na^+Cl^- ions (150 mM) were added to the simulation systems with access Na^+ ions to compensate for the net negative charge of the MHC molecules.

The OPLS all-atom forcefield was applied (16).

All MD simulations were carried out using the Gromacs simulation suite (17). Application of the Lincs (18) and Settle (19) methods allowed for an integration step size of 2 fs. Short range electrostatic interactions (distance <1 nm) between charge groups were calculated explicitly, and long range electrostatic interactions were calculated using the Particle-Mesh Ewald Method (20). The systems were coupled to an external temperature bath (21) of 310 K with a coupling time constant of $\tau_T = 0.01$ ps separately for the protein and the solvent (including ions). The pressure was kept constant by a weak coupling to a pressure bath (21) with $\tau_P = 1$ ps. Each simulation started with an energy minimization using a steepest descent algorithm (1000 steps) and was followed by simulations of 100-ps length with harmonic position restraints applied on all heavy protein atoms (force constant: 1000 kJ/mol/nm²) to allow relaxation of the solvent molecules.

Estimation of Peptide Entropy from MD Simulation—The entropy of the m9 peptide bound to the MHC is estimated based on a quasi-harmonic approximation of the absolute entropy (22). The entropy $S = -k_B\langle\ln\rho\rangle$ with the probability distribution ρ for a harmonic oscillator is shown to yield an upper bound for the true entropy of the system. The generalization for many degrees of freedom reads
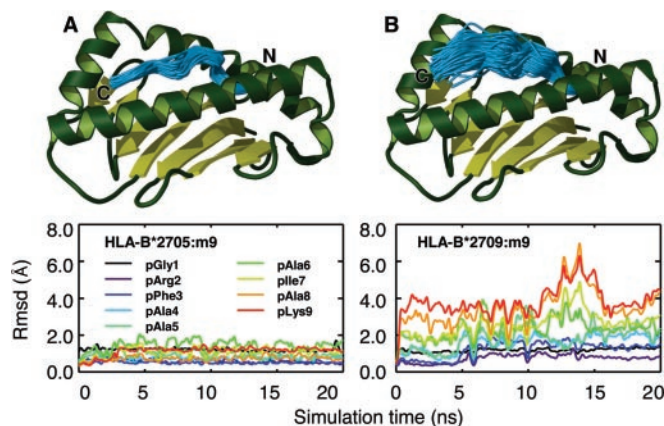
FIG. 2. **Subtype-dependent conformational heterogeneity.** Peptide binding groove (1–180) of the HLA-B*2705 (*A*) and of the HLA-B*2709 (*B*) subtypes together with 200 snapshots of the m9 peptide sampled over the respective 20 ns simulations. The *lower row* shows the root mean square deviation (*Rmsd*) values (averaged over backbone atoms) color-coded separately for the nine peptide amino acids as a function of simulation time after fit to the peptide binding groove.

$$S = k_B \frac{\gamma}{e^\gamma - 1} - k_B \ln(1 - e^{-\gamma}) \qquad \text{(Eq. 6)}$$

with

$$\gamma = \frac{h}{2\pi} \frac{\sqrt{\beta}}{\sqrt{\sigma}} \qquad \text{(Eq. 7)}$$

where σ denotes the mass-weighted covariance matrix,

$$\sigma_{ik} = \sqrt{m_i m_k} \langle (x_i - \langle x_i \rangle)(x_k - \langle x_k \rangle) \rangle \qquad \text{(Eq. 8)}$$

which is computed from the MD trajectories.

RESULTS AND DISCUSSION

The dynamics and motional freedom of the bound m9 peptide, as well as the thermodynamic stability of the two differentially autoimmune disease-associated HLA-B27-subtypes B*2705 and B*2709 complexed with m9, were probed by time-resolved fluorescence depolarization using the fluorescent reporter group Lucifer Yellow iodoacetamide (LYIA) covalently bound to a cysteine introduced at position 6 of the m9 peptide (m9-C6-LY). Rotational correlation times of peptide motion were extracted from time-resolved fluorescence anisotropy decays (Fig. 1, *A–C*, and supplemental Table S1). The anisotropy decay of the fluorescent peptide complexed with the HLA-B27 subtypes at 20 °C (Fig. 1B) can be best fitted by three correlation times, one reflecting the motion of the fluorescent dye (~0.2 ns), a 2-ns component assigned to the bound peptide (described below), and a longer correlation time (~17 ns) corresponding to the rotational motion of the whole complex. The fastest rotational correlation time (0.2 ns) agrees well with the rotational correlation time of Lucifer Yellow in solution (0.14 ns) (Fig. 1A). The size of the molecule estimated from the viscosity dependence of the slowest rotational correlation time under the assumption of a spherical rotator yields an effective hydrodynamic diameter of $d = 57 \pm 3$ Å for both subtypes, in very good agreement with the average diameter of about 60 Å obtained from the crystal structures (Fig. 1D) (11). This result suggests that under our experimental conditions B*2705 and B*2709 complexes exist in a monomeric rather than in an oligomeric form (23). The assignment of the fastest and slowest of the three rotational correlation times to the motion of the fluorescent dye itself and the whole complex, respectively, leaves only the 2-ns component (at 20 °C) for the dynamics of the peptide. This correlation time is slower than the rotational correlation time of the peptide free in solution (0.64 ± 0.03 ns;
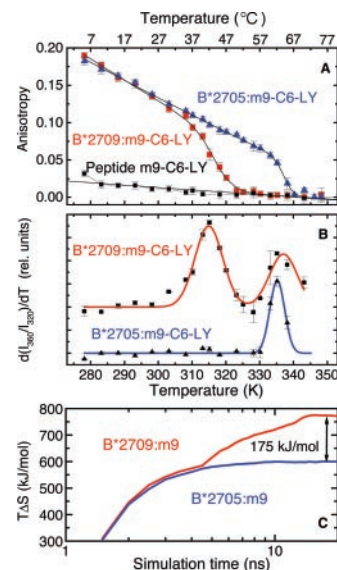
FIG. 3. **Thermal denaturation curves and configurational entropic energy.** *A*, thermal dissociation of the peptide m9-C6-LY from B*2705 (*blue*) and B*2709 (*red*) and fit to Equation 4 (Table 1). *Error bars* represent at least five different measurements. Conditions were the same as described in the legend to Fig. 1, *A–C*. *B*, first derivatives of thermal denaturation curves of B*2705:m9-C6-LY (*blue*) and B*2709:m9-C6-LY (*red*) from the change in tryptophan fluorescence at 360 nm normalized to the intensity changes at 320 nm. Excitation was at 280 nm. *C*, configurational entropic energy at 310 K (37 °C) of m9 as a function of simulation time. The entropy appears to be converged within 9 ns (B*2705) or 15 ns (B*2709).

Fig. 1A and supplemental Table S1), likely due to interaction with the binding groove.

At 20 °C no significant difference was seen between the two subtypes (Fig. 1B). However, the respective peptide dynamics shows pronounced differences at physiological temperature (Fig. 1C). Specifically, the peptide in the binding groove of the HLA-B*2709 subtype is more flexible than in B*2705:m9 as evidenced by the faster rotational correlation time of the peptide component with $\phi_2 = 1.1 \pm 0.2$ ns (B*2709:m9-C6-LY) compared with $\phi_2 = 1.60 \pm 0.03$ ns (B*2705:m9-C6-LY).

To obtain an atomistic interpretation of the measured enhanced mobility of the peptide we performed extended MD simulations of B*2705 and B*2709 with bound m9 (Fig. 2). Indeed, the m9 peptide displays a dramatically enhanced flexibility when bound to B*2709, as can be seen from representative snapshots of the m9 conformations (Fig. 1, *E* and *G*). The different conformational ensembles sampled by the peptide in the simulations are depicted in Fig. 2. Whereas the conformational bundle is narrow in B*2705 (Fig. 2A, *top*), the simulations yield an exceptionally broad distribution of m9 conformations in the B*2709 subtype (Fig. 2B, *top*). The subtype-dependent conformational heterogeneity increases toward the C terminus of the peptide (compare Fig. 2, top), with main chain atoms of pLys-9 and pAla-8 showing deviations of up to 7 Å around the B*2709 x-ray conformation, whereas the corresponding value for B*2705 is less than 2 Å (Fig. 2, *bottom*). Thus, in the simulations at 310 K, the peptide bound to B*2709 gets partially untrapped at the C terminus. This contrasts with the small deviations (maximum 0.6 Å) of peptide residues between the crystal structures of the two subtypes, which were, however, obtained at 100 K (11). Unlike the C terminus, the primary anchor residue pArg-2, which is common among HLA-B27 subtypes, remains tightly bound in both simulations.

The increase in peptide flexibility can be quantified by the root mean square fluctuations. The root mean square fluctua-

TABLE I
Thermal peptide dissociation and pMHC melting parameters

Conditions: 10 mM sodium phosphate buffer, pH 7.5, 150 mM NaCl.

Sample	$T_m{}^a$	$T_m{}^b$	$\Delta H°$	$\Delta S°$
	°C	°C	kJ mol^{-1}	kJ mol^{-1} K^{-1}
B*2705-**m9**-C6-LY^c	65.3 ± 1.4	64 ± 2	647 ± 39	1.91 ± 0.12
B*2705-**TIS**-C6-LY^d	58.1 ± 0.5		393 ± 27	1.16 ± 0.13
B*2705-**pVIPR**-C8-LY^e	61 ± 1		468 ± 1	1.40 ± 0.03
B*2709-**m9**-C6-LY^c	45.8 ± 2.3	44 ± 3; 62 ± 3	290 ± 14	0.91 ± 0.05
B*2709-**TIS**-C6-LY^d	60.1 ± 0.5		346 ± 111	1.04 ± 0.33
B*2709-**pVIPR**-C8-LY^e	52 ± 1		326 ± 1	1.00 ± 0.03

^{a} Results from peptide unbinding as measured by steady-state fluorescence polarization of the LY-labeled peptide.

^{b} Results from overall complex denaturation as measured by the change in fluorescence intensity at the blue (320 nm) and red (360 nm) side of the tryptophan emission band.

^{c} Average of two independent measurements. The S.D. values are given.

^{d} Average of three independent measurements. The S.D. values are given.

^{e} One measurement. The S.D. values of the fit are given.

tion of pAla-6 (Fig. S4), the attachment position of the fluorescent dye, is 1.24 ± 0.05 Å in B*2709:m9, compared with 0.71 ± 0.03 Å in B*2705:m9, when averaging over 1-ns trajectory sections.

Fig. 1*E* shows three representative conformations of the B*2709-bound m9 peptide (*blue*, occupation (*oc*) 66%; *green*, occupation 25%; and *red*, occupation 9%) sampled in the simulation (Fig. 2B), derived from a principal component analysis (24) (Fig. 1*F*), and the crystal conformation found in B*2709:m9 (*gray*). In addition to the large shift in the C-terminal pLys-9 with respect to the crystal conformation, we identified two conformations for pPhe-3 (Fig. 1*e*, *blue/red* and *green*). However, the salt bridge of pLys-9 to Asp-77 of the α1-helix is only broken for one of the three peptide conformations (Fig. 1E, *red*). This conformation is stabilized by a hydrogen bond between pAla-6 and Gln-155. In addition, a hydrogen bond between Lys-146 and the carboxyl oxygen of pLys-9 is retained. Thereby, pLys-9 imposes an increased flexibility also on the N-terminal part of the α2-helix (residues 137–150). A higher mobility of this domain is also seen in simulations of peptide-free HLA-B27 subtypes (data not shown) and in a normal mode analysis of peptide-free HLA-A2 molecules (25). This suggests that the flexibility of the α2-helix in B*2705:m9 is restricted by firm anchoring of the pLys-9 side chain to the floor of the binding groove (Asp-116). This type of anchoring cannot be realized between pLys-9 and His-116 in B*2709:m9, which contributes to the observed flexibility. Several residues in the α2-helix including Lys-146 are highly conserved among HLA-A, -B, and -C antigens (26), in line with the importance of this region for TCR binding (5, 6).

The different flexibilities of the peptide and its binding grooves, as seen both in the simulations and in the time-resolved experiments, explain the measured entropy changes for the thermally induced peptide dissociation (Fig. 3*A*). Assuming a two-state reaction, the steady-state anisotropy data in Fig. 3*A* yield the enthalpy change, ΔH^0, and entropy change, ΔS^0, for peptide unbinding (Table I). The transition temperatures for m9 dissociation with 46 ± 2 °C (B*2709) and 65 ± 1 °C (B*2705) (Fig. 3, *A* and *B*, and Table I), match those of the unfolding of the whole complex as deduced from the change in fluorescence intensity of the tryptophan emission band (Fig. 3*B*). The second peak observed for B*2709:m9 (Fig. 3*B*) is due to β2m unfolding (14, 27). At physiological temperature, the difference in $T\Delta S^0$ between the subtypes is 311 ± 20 kJ/mol, reflecting the entropic difference between B*2705 and B*2709 complexed with m9.

This difference in entropy is further explained by the simulations, from which the entropic contribution of the peptide was estimated using a quasi-harmonic approximation (22). In the non-disease-associated B*2709 subtype, the entropic energy of

m9 at physiological temperature is higher than in B*2705 by $T\Delta S$ = 175 kJ/mol (Fig. 3*C*), which is about 60% of the measured change. We attribute the remaining 40% of the loss in entropy upon peptide binding to the peptide-induced immobilization of the binding groove.

These results suggest an entropic control of peptide presentation. In particular, our study shows that virtually identical pMHC crystal structures (11) can exhibit drastic HLA subtype-dependent *dynamical* differences, even though the subtypes are distinguished only by a deeply buried polymorphism. This differential flexibility of the HLA-B27 subtypes is due to a complex interplay between residue 116 polymorphism and the peptide displayed (Figs. 1*C* and 2 and Table I). It is tempting to speculate that also the binding of TCR or other ligands on an effector cell to a pMHC must at least partly be controlled by the observed pMHC flexibility, influencing effector cell responses (3).

To test this entropic control hypothesis, we obtained thermodynamic data also for two additional peptides, TIS (RRLPIF-SRL) and pVIPR (RRKWRRWHL) (28, 29). Strikingly, for both LY-labeled self-peptides the change in entropy upon peptide dissociation from B*2709 is close to that for m9, whereas for the disease-associated subtype B*2705 the entropy changes are peptide-dependent (Table I). The increased thermal stability of B*2705:pVIPR compared with B*2709:pVIPR is in agreement with the recently resolved crystal structures of B*2705:pVIPR and B*2709:pVIPR (30), which show two distinct conformations of pVIPR. The non-conventional p6α conformation with an additional salt bridge between pArg-5 and Asp-116 was only observed for B*2705:pVIPR, suggesting an increased stability of this complex with respect to B*2709:pVIPR. As the entropy changes for B*2705 are never smaller than the corresponding values for B*2709, they imply MHC polymorphism-linked entropic thresholds, which distinguish peptide presentation by the two subtypes (Table I and Fig. 3).

In the case of HLA-B27, the existence of such entropic thresholds between the disease-associated and the non-associated subtype (Table I and Fig. 3) points to a possible connection with AS pathogenesis through differential development of HLA-B27-restricted T-cell repertoires in B*2705- and B*2709-positive individuals (29, 30). Distinct repertoires against the self-peptide pVIPR have already been shown to exist in individuals with B*2705 or B*2709, respectively (29). pVIPR evokes a specific cytotoxic T-cell (CTL) response that is higher in B*2705-positive AS patients than in healthy B*2705 controls, while such CTL responses have so far not been found in persons who are positive for B*2709. Subtype-dependent differential peptide dynamics might also be connected to the pathogenesis of other disease states. For example, the rate of progression to AIDS in human immunodeficiency virus-posi-

tive patients (31) or the outcome of bone marrow transplants between unrelated individuals (32) are both associated with residue 116 polymorphism. Thus, the dissection of the subtype-dependent peptide flexibilities provides a dynamical framework for unraveling the link between a class I molecule, *e.g.* HLA-B27, and autoimmune diseases.

Taken together, our results demonstrate that the bound peptide and surrounding heavy chain residues in class I molecules exhibit a wide range of flexibilities, which are linked to MHC polymorphism. Enhanced peptide flexibilities, however, do not necessarily influence peptide binding affinities (33). Recent findings suggest that peptide residues are mainly involved in pMHC-TCR complex stabilization, allowing efficient T-cell activation (34). However, an optimal dwell-time range for the interaction of TCR and pMHC is crucial as well (3, 4). In addition, a role of entropic effects for TCR binding has been assumed (35). From x-ray crystallographic studies on bound and unbound states of the TCR (36, 37) and thermodynamic data, it was suggested that the loss in entropy upon binding was mainly due to pronounced conformational differences observed in the loops of TCR complementarity-determining regions (35). Our results, however, demonstrate that also the bound peptide and surrounding heavy chain residues may exhibit pronounced flexibility. By entropically contributing to ligand binding and unbinding kinetics, the degree of pMHC flexibility can in particular control optimal T-cell recognition and activation via the half-life of the pMHC-TCR interaction (3–5, 34–36). We propose this entropic mechanism as the atomistic basis for the control of pMHC recognition.

REFERENCES

1. Madden, D. R. (1995) *Annu. Rev. Immunol.* **13,** 587–622
2. Mason, D. (1998) *Immunol. Today* **19,** 395–404
3. Krogsgaard, M., Prado, N., Adams, E. J., He, X., Chow, D., Wilson, D. B., Garcia, K. C., and Davis, M. M. (2003) *Mol. Cell* **12,** 1367–1378
4. Kalergis, A. M., Boucheron, N., Doucey, M. A., Palmieri, E., Goyarts, E. C., Vegh, Z., Luescher, I. F., and Nathenson, S. G. (2001) *Nat. Immunol.* **2,** 229–234
5. Rudolph, M. G., Luz, J. G., and Wilson, I. A. (2002) *Annu. Rev. Biophys. Biomol. Struct.* **31,** 121–149
6. Housset, D., and Malissen, B. (2003) *Trends. Immunol.* **24,** 429–437
7. Ding, Y.-H., Baker, B. M., Garboczi, D. N., Biddison, W. E., and Wiley, D. C. (1999) *Immunity* **11,** 45–56
8. Bankovich, A. J., and Garcia, K. C. (2003) *Immunity* **18,** 7–11
9. Degano, M., Garcia, K. C., Apostolopoulos, V., Rudolph, M. G., Teyton, L., and Wilson, I. A. (2000) *Immunity* **12,** 251–261
10. Ramos, M., and López de Castro, J. A. (2002) *Tissue Antigens* **60,** 191–205
11. Hülsmeyer, M., Hillig, R. C., Volz, A., Ruhl, M., Schroder, W., Saenger, W., Ziegler, A., and Uchanska-Ziegler, B. (2002) *J. Biol. Chem.* **277,** 47844–47853
12. Alexiev, U., Rimke, I., and Pöhlmann, T. (2003) *J. Mol. Biol.* **328,** 705–719
13. Eftink, M. R. (1994) *Biophys. J.* **66,** 482–501
14. Hillig, R. C. Hülsmeyer, M., Saenger, W., Welfle, K., Misselwitz, R., Welfle, H., Kozerski, C., Volz, A., Uchanska-Ziegler, B., and Ziegler, A. (2004) *J. Biol. Chem.* **279,** 652–663
15. Jorgensen, W. L., Chandrasekhar, J., and Madura, J. D. (1983) *J. Chem. Phys.* **79,** 926–935
16. Kaminski, G., Friesner, R. A., Tirado-Rives, J., and Jorgensen, W. L. (2001) *J. Phys. Chem. B* **105,** 6474–6487
17. Lindahl, E., Hess, B., and van der Spoel, D. (2001) *J. Mol. Model.* **7,** 306–317
18. Hess, B., Bekker, H., Berendsen, H. J. C., and Fraije, J. G. E. M. (1997) *J.Phys. Comp.* **18,** 1463–1472
19. Miyamoto, S., and Kollman, P. A. (1992) *J. Comp. Chem.* **13,** 952–962
20. Darden, T., York, D., and Pedersen, L. (1993) *J. Chem. Phys.* **98,** 10089–10092
21. Berendsen, H. J. C., Postma, J. P. M., van Gunsteren, W. F., DiNola, A., and Haak, J. R. (1984) *J. Chem. Phys.* **81,** 3684–3690
22. Schlitter, J. (1993) *Chem. Phys. Lett.* **215,** 617–621
23. Gakamsky, D. M., Haas, E., Robbins, P., Strominger, J. L., and Pecht, I. (1995) *Immunol. Lett.* **44,** 195–201
24. Amadei, A., Linssen, A. B. M., and Berendsen, H. J. C. (1993) *Proteins* **17,** 412–425
25. Nojima, H., Takeda-Shitaka, M., Kurihara, Y., Kamiya, K., and Umeyama, H. (2003) *Chem. Pharm. Bull.* **51,** 923–928
26. Reche, P. A., and Reinherz, E. L. (2003) *J. Mol. Biol.* **331,** 623–641
27. Bouvier, M., and Wiley, D. C. (1994) *Science* **265,** 398–402
28. Fiorillo, M. T. Greco, G., Maragno, M., Potolicchio, I., Monizio, A., Dupuis, M. L., and Sorrentino, R. (1998) *Eur. J. Immunol.* **28,** 2508–2516
29. Fiorillo, M. T., Maragno, M., Butler, R., Dupuis, M. L., and Sorrentino, R. (2000) *J. Clin. Invest.* **106,** 47–53
30. Hülsmeyer, M., Fiorillo, M. T., Bettosini, F., Sorrentino, R., Saenger, W., Ziegler, A., and Uchanska-Ziegler, B. (2004) *J. Exp. Med.* **199,** 271–281
31. Gao, X., Nelson, G. W., Karacki, P., Martin, M. P., Phair, J., Kaslow, R., Goedert, J. J., Buchbinder, S., Hoots, K., Vlahov, D., O'Brien, S. J., and Carrington, M. (2001) *N. Engl. J. Med.* **344,** 1668–1675
32. Ferrara, G. B., Bacigalupo, A., Lamparelli, T., Lanino, E., Delfino, L., Morabito, A., Parodi, A. M., Pera, C., Pozzi, S., Sormani, M. P., Bruzzi, P., Bordo, D., Bolognesi, M., Bandini, G., Bontadini, A., Barbanti, M., and Frumento, G. (2001) *Blood* **98,** 3150–3155
33. de Haan, E. C., Wauben, M. H. M., Grosfeld-Stulemeyer, M. C., Kruijtzer, J. A. W., Liskamp, R. M. J., and Moret, E. E. (2002) *Bioorg. Med. Chem.* **10,** 1939–1945
34. Wu, L. C., Tuot, D. S., Lyons, D. S., Garcia, K. C., and Davis, M. M. (2002) *Nature* **418,** 553–556
35. Willcox, B. E., Gao, G. F., Wyer, J. R., Ladbury, J. E., Bell, J. I., Jakobson, B. K., and van der Merve, P. A. (1999) *Immunity* **10,** 357–365
36. Garcia, K. C., Degano, M., Pease, L. R., Huang, M., Peterson, P. A., Teyton, L., and Wilson, I. A. (1998) *Science* **279,** 1166–1172
37. Reiser, J.-B., Gregoire, C., Darnault, C., Mosser, T., Guimezanes, A., Schmitt-Verhulst, A. M., Fontecilla-Camps, J. C., Mazza, G., Malissen, B., and Housset, D. (2002) *Immunity* **16,** 345–354